



1 Improvement in tropospheric moisture retrievals from VIIRS 2 through the use of infrared absorption bands constructed from 3 VIIRS and CrIS data fusion

4 E. Eva Borbas¹, Elisabeth Weisz¹, Chris Moeller¹, W. Paul Menzel¹, Bryan A. Baum²

5 ¹Cooperative Institute for Meteorological Satellite Studies, University of Wisconsin-Madison, Madison, Wisconsin,
6 USA

7 ²Science and Technology Corporation, Madison, Wisconsin, USA

8 *Correspondence to:* E. Eva Borbas (eva.borbas@ssec.wisc.edu)

9 **Abstract.** An operational data product available for both the Suomi-NPP and NOAA-20 platforms provides high
10 spatial resolution infrared (IR) absorption band radiances for VIIRS based on a VIIRS+CrIS data fusion method. This
11 study investigates the use of these IR radiances, centered at 4.5, 6.7, 7.3, 9.7, 13.3, 13.6, 13.9, and 14.2 μm , to construct
12 atmospheric moisture products (e.g., total precipitable water and upper tropospheric humidity) and to evaluate their
13 accuracy. Total precipitable water (TPW) and upper tropospheric humidity (UTH) retrieved from hyperspectral
14 sounder CrIS measurements are provided at the associated VIIRS sensor's high spatial resolution (750m) and are
15 compared subsequently to collocated operational Aqua MODIS and Suomi-NPP VIIRS moisture products. This study
16 suggests that the use of VIIRS IR absorption band radiances will provide continuity with Aqua MODIS moisture
17 products.

18 1. Introduction

19 Retrieval of atmospheric water vapor properties from the Visible Infrared Imaging Radiometer Suite (VIIRS) satellite
20 sensor on the Suomi National Polar-orbiting Partnership (S-NPP) and the National Oceanic and Atmospheric
21 Administration (NOAA-20) platforms is challenging due to the absence of infrared (IR) water vapor absorption bands.
22 Fortunately, measurements in the missing spectral region are available on the Crosstrack Infrared Sounder (CrIS), a
23 hyperspectral IR sensor also on the same platforms. Spectral measurements in these IR absorption bands can be
24 constructed for VIIRS through fusion of the imager and sounder data. Weisz et al. (2017) demonstrated a fusion
25 method to construct IR water vapor and carbon dioxide absorption band radiances for VIIRS at 750m spatial
26 resolution. With the addition of the missing spectral bands to VIIRS on Suomi-NPP, this study evaluates Total column
27 Precipitable Water vapor (TPW) and Upper Tropospheric Humidity (UTH) in clear skies through comparison to the
28 MODerate resolution Imaging Spectroradiometer (MODIS) MYD08 (Platnick et al., 2013) Collection 6.1 and Version
29 1.0 VIIRS (Borbas et al., 2019a-d) atmospheric products. The water vapor product shows improvement with the use
30 of these constructed band radiances, with the major improvement being found in the tropics.

31

32 While VIIRS has a wide scanning swath, high horizontal resolution, a nearly constant pixel size across the scan, and
33 a day/night band (DNB), it's spectral complement lacks thermal infrared (IR) absorption bands necessary to accurately



1 retrieve tropospheric moisture content as well as cloud properties that rely on those spectral measurements. In
2 particular for moisture determinations, VIIRS does not take measurements in the broad 6.7- μm water vapor band that
3 are measured by the MODIS (Seemann et al., 2003). Fortunately, the missing IR spectral bands can be gleaned from
4 measurements on the companion hyperspectral CrIS sensor on the same platform.

5
6 Here we denote the instantaneous field of regard as field-of-view (FOV) for the sounder and pixel for the imager
7 exclusively to minimize confusion between the two sensors. To achieve TPW and UTH at imager pixel resolution,
8 this study employs the innovative data fusion approach of Weisz et al. (2017) that constructs MODIS-like water vapor
9 and CO_2 sensitive radiances directly at the imager resolution through use of co-located VIIRS and CrIS radiances. In
10 this study, the data fusion method provides MODIS-like IR absorption band radiances at the VIIRS M-band spatial
11 resolution (750m). The VIIRS+CrIS fusion radiances are available for the entire record of both S-NPP and NOAA-
12 20 platforms (Baum et al., 2019a).

13
14 The availability of these IR-band radiances for VIIRS at 750m pixel resolution makes it possible to retrieve a cloud
15 mask and moisture properties using algorithms developed and tested using the full MODIS spectral band suite (Borbas
16 et al., 2011). The goal of this study is to determine the impact of supplementing VIIRS with imager-resolution
17 VIIRS+CrIS fusion bands on retrieving TPW and UTH. This paper is organized as follows: Section 2 discusses data
18 and fusion method; Section 3 summarizes the moisture retrieval method and presents results, and a summary of the
19 findings is provided in Section 4.

20 **2. Data and Methodology**

21 The VIIRS sensor is a 22-band scanning radiometer that is currently flying on the NASA Suomi NPP and the NOAA-
22 20 platforms. VIIRS has 16 bands scanning a 3000 km swath at 750m resolution (medium resolution, or M), 5 bands
23 at 375m resolution (imaging, or I), and a day/night band. For this investigation, the focus is on using the bands at M
24 resolution. The data used in this study include the standard Level-1B VIIRS data for both the S-NPP and NOAA-20
25 platforms made available by the Atmosphere Science Investigator-led Processing System (A-SIPS) located at the
26 University of Wisconsin–Madison Space Science Engineering Center (SSEC).

27
28 The Cross-track Infrared Sounder (CrIS) is a Fourier transform spectrometer with 1305 spectral channels in normal
29 spectral resolution (NSR) and 2211 channels in full spectral resolution (FSR) over 3 wavelength ranges: LWIR (9.14-
30 to 15.38- μm); MWIR (5.71- to 8.26- μm); and SWIR (3.92- to 4.64- μm). CrIS scans a 2200 km swath width (\pm 50
31 degrees), with 30 Earth-scene views. Each view consists of 9 FOVs from a 3x3 array that have a nadir spatial resolution
32 of approximately 14 km.

33
34 The fusion method requires an accurate co-location between the high spatial resolution imager data (with pixels at
35 750m) and the lower-spatial-resolution sounder data (with FOVs at about 14 km). The fusion method described in

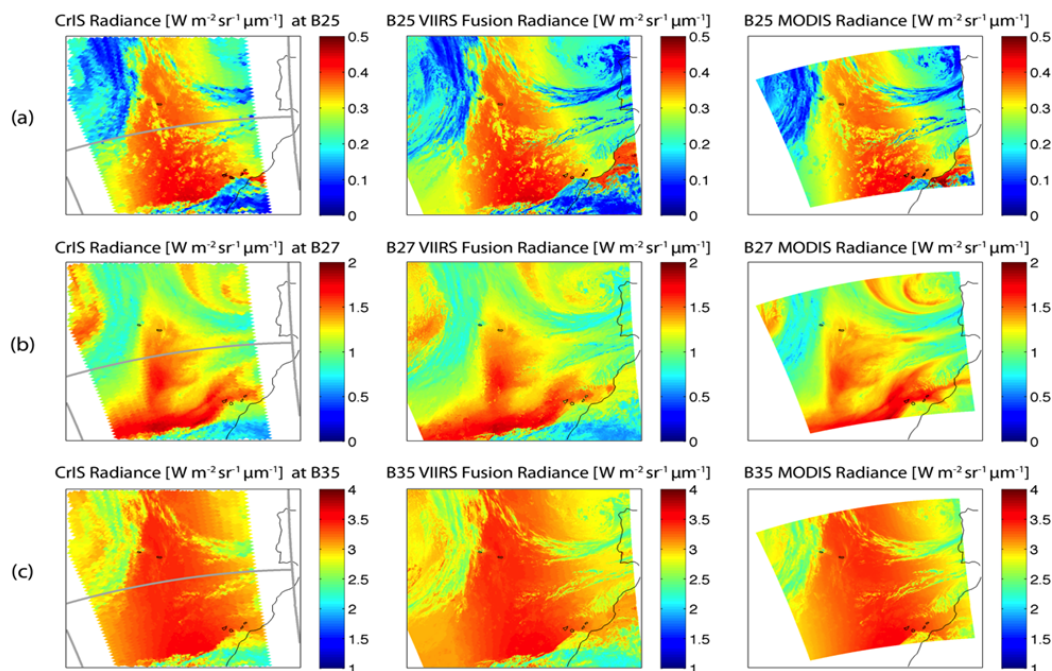


1 Weisz et al. (2017) consists of two steps for each imager pixel: (a) Search nearby neighbors to find the five best
2 matching split window FOVs to the chosen pixel split window measurements – this is accomplished using a k - d tree
3 search algorithm on both high spatial (M-band data) and low spatial (M-band data averaged over the CrIS FOV)
4 resolution split-window (11 and 12- μ m) imager radiances. (b) Convolve the high spectral sounder radiances (at low
5 spatial resolution) to the desired IR broadband; then average the convolved sounder radiances associated with the
6 selected five nearest neighbors to construct the desired spectral band for each imager pixel. Spectral radiance
7 convolution refers to the process of converting high spectral resolution (narrowband) to broadband radiance
8 measurements by applying a spectral response function (SRF) of a given broadband. Here, SRFs associated with the
9 spectral bands of the MODIS sensor on the NASA Earth Observation system (EOS) Aqua platform are applied to
10 CrIS measurements. The VIIRS+CrIS fusion IR absorption band radiances are available for the entire records of S-
11 NPP and NOAA-20 at the Level-1 and Atmosphere Archive and Distribution System (LAADS) Distributed Active
12 Archive Center (DAAC) at NASA Goddard Space Flight Center (Baum et al., 2019a, b).

13

14 VIIRS+CrIS fusion radiances alongside observed radiances for MODIS bands 25 (4.5 μ m), 27 (6.7 μ m) and 35 (13.9
15 μ m), repeated from Weisz et al. (2017), are shown in Fig. 1. The fusion results for band 27 show more inaccuracies,
16 because H₂O-sensitive spectral bands sense different tropospheric regions than split-window spectral bands. Also,
17 small-scale and narrow spatial features in moisture (e.g., dry slots and cloud edges), which are not captured by the
18 sounder due to its large spatial resolution, are more problematic for the fusion process. Furthermore, the results at the
19 edge of the imager granule (i.e., outside the sounder swath) should be used with caution since they do not account for
20 “limb darkening” and hence tend to be less accurate. Results shown in Fig. 1 for the VIIRS+CrIS fusion radiances
21 compared well in a qualitative sense with the observed MODIS radiances, even in the more challenging water vapor
22 band.

23



1

2 **Figure 1.** CrIS sounder radiance (left), newly constructed fusion radiance (middle), and the observed MODIS radiance
3 differences (right) for MODIS bands 25 (4.5 μm), 27 (6.7 μm) and 35 (13.9 μm) in panels a, b and c, respectively, for one
4 granule at 1436 UTC on April 17, 2015. This is shown as Figure 8 in Weisz et al. (2017).

5

6

7 To assess the viability of the moisture products to provide continuity with similar products from MODIS, we perform
8 a comparison with co-located measurements (i.e., matchups) with Aqua MODIS. For this study, the co-location
9 process requires the VIIRS 750m pixel to be fully contained within the MODIS 1-km pixel; the scene must be high
10 confidence clear (as identified by the MODIS cloud mask MYD35); and the scan angles for the matching pair must
11 be less than 50° . Figure 2 shows the results of tens of thousands of instances of collocated MODIS and VIIRS+CrIS
12 fusion radiances that are converted to brightness temperatures (BTs) in two water vapor and four carbon dioxide bands
13 for the month of April 2018. It can be seen that the mean clear-sky brightness temperature differences (BTDs) between
14 VIIRS+CrIS fusion and original MODIS data are less than 0.5 K for MODIS H₂O bands 27 to 28 (6.7 and 7.3 μm)
15 and MODIS CO₂ bands 33 to 36 (13.3, 13.6, 13.9, and 14.2 μm) for 11- μm BTs ranging from 200 to 280 K. In
16 summary, an order of magnitude spatial resolution (from 14 km to 750 m) has been added at the cost of increasing
17 measurement noise by 0.25 to 0.5 K. Results for all twelve months in 2018 (not shown) are similar; in fact, results
18 for the entire S-NPP archive show comparably positive fusion results.

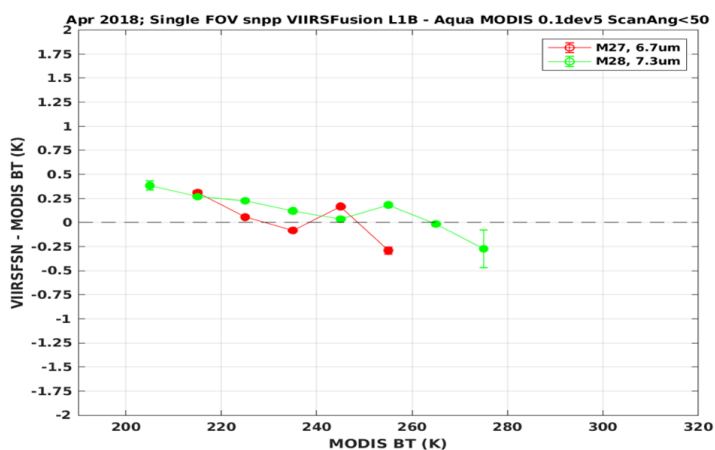
19

20

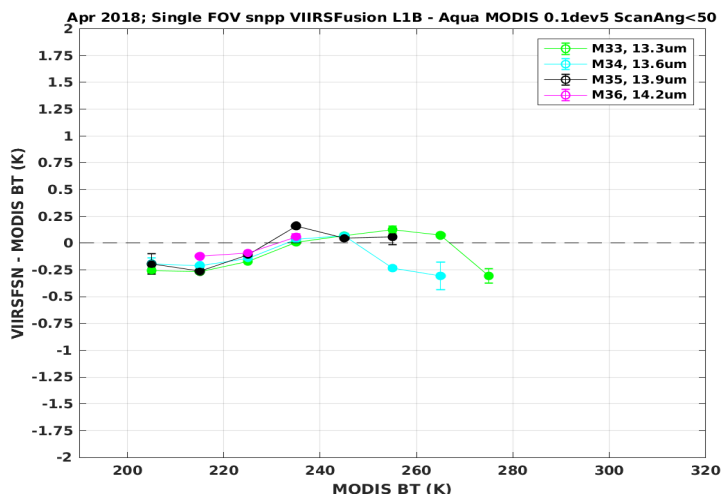
21



(a)



(b)



1 Figure 2. Comparison of collocated MODIS and VIIRS/CrIS fusion water vapor (a) and carbon dioxide (b) band brightness
2 temperatures for the month of April 2018. Each data point in the plots (within a ten-degree brightness temperature bin)
3 represents more than ten thousand collocations.

4 3. TPW and UTH Algorithm and Results

5 Our retrieval of TPW and UTH from selected IR measurements adopts a statistical regression algorithm (Seemann et
6 al. 2003 and 2008; Li et al., 2000; Smith and Woolf, 1988; Hayden 1988) performed using clear sky radiances (and
7 BTs) measured over land and ocean for both day and night. The regression is developed with the SeaBor training
8 database (Borbas et al., 2005) that consists of over 15,000 atmospheric profiles globally and seasonally well
9 distributed. The water vapor retrieval algorithm has two parts, first the regression coefficients are calculated using
10 radiative transfer calculations, and then the regression retrieval is performed. The radiative transfer calculation of the
11 MODIS-like radiances of bands 25, 27, 28 and 30-36 is performed using the forward model called Radiative Transfer



1 for TOVS (RTTOV) Version 12 (Saunders et al., 2018). The regression relationships between the calculated BTs and
2 retrieved moisture products are generated for four (and three) different BT zones over land and ocean, respectively,
3 and 60 sensor zenith angles from nadir to 60°. The only other ancillary information required is the surface pressure,
4 which is provided by NCEP Reanalysis data (Saha et al., 2010). TPW and UTH are determined for clear sky radiances
5 measured by VIIRS and calculated from VIIRS+CrIS fusion. The retrieval approach is similar to that adopted for
6 MODIS. There is a strong reliance on radiances from 6.7, 11, and 12 μm . The operational VIIRS cloud mask (called
7 CLDMSK_L2_VIIRS_SNPP.001, Ackerman et al., 2019) is applied to VIIRS to characterize the probability of cloud
8 cover.

9

10 Figure 3 shows CrIS TPW and UTH at the sounder FOV resolution; they outline the tropospheric moisture gradients
11 at coarse ($\sim 14\text{km}$) resolution for clear and partly cloudy skies. The soundings are obtained using the Dual Regression
12 method (Smith et al. 2012, Weisz et al., 2013) which is a computationally fast, physically-based method that retrieves
13 profiles as well as surface and cloud properties from high spectral resolution radiances measured in both clear and
14 cloudy-sky conditions at single FOV resolution. TPW represents the total column integration of the moisture profile
15 while UTH is the integration from 400 hPa to the top of the atmosphere. Also shown are the regression retrieval
16 results for the VIIRS+CrIS fusion spectral band radiances (created using the MODIS-like IR spectral response
17 functions) at higher spatial resolution ($\sim 750\text{m}$) in pixels deemed to be clear in the VIIRS cloud mask. They display
18 more refined features and improve the coverage, but show higher values of TPW off the coast of Baja and miss some
19 of the UTH features in Wyoming and Colorado suggested in the CrIS soundings. While the results are derived from
20 two independent algorithms, this example illustrates a challenge for the VIIRS split window search for nearby FOVs;
21 the search will rely primarily on low level temperature and moisture features and less on mid to upper level moisture
22 gradients.

23

24

25

26

27

28

29

30

31

32

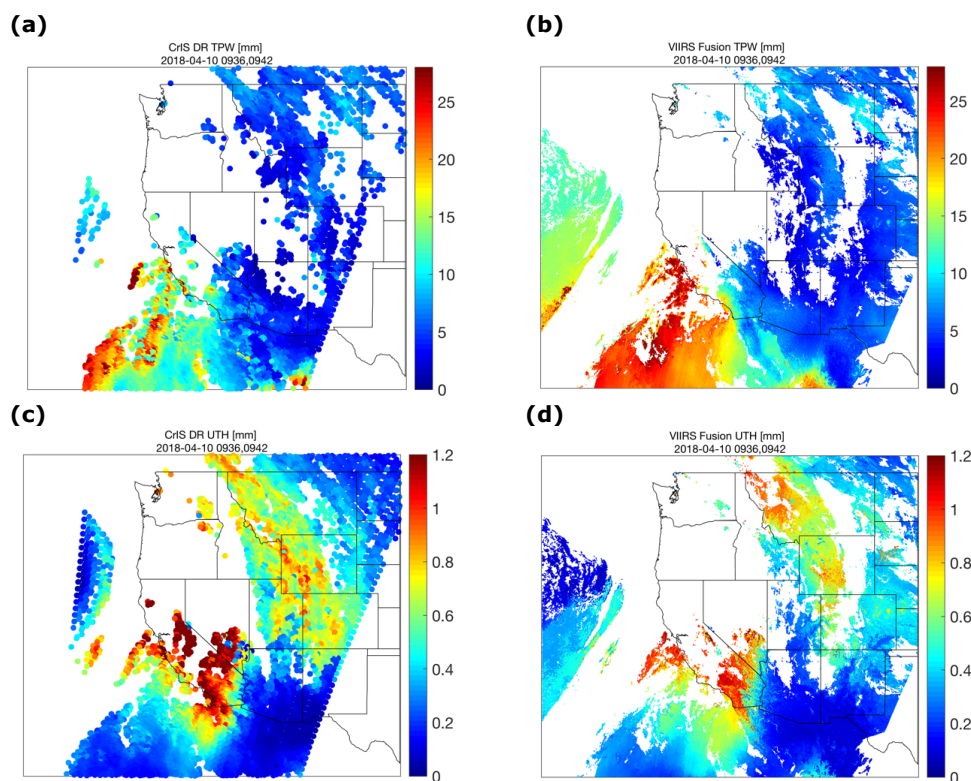
33

34

35

36

37



1 Figure 3. TPW (a,b) and UTH (c,d) (both in mm) are shown for CrIS DR retrievals at sounder resolution (a,c) along with
2 regression retrievals derived from VIIRS+CrIS fusion radiances at imager resolution (b,d) for 10 April 2018, at 0936 and
3 0942 UTC (CrIS granule start times).

4

5 3a. TPW Results

6 A one-day evaluation of the VIIRS+CrIS TPW fusion product is shown in Fig. 4. Global comparisons for 9 April
7 2018 are made for the TPW field derived from (1) VIIRS+CrIS fusion radiances using the operational MODIS L2
8 algorithm, (2) MODIS operational Col 6.1 MYD08 (MYD08_D3.006, Platnick et al., 2015), (3) VIIRS-only (Borbás
9 et al., 2019d), and (4) the VIIRS+NUCAPS (Borbás et al., 2019d) operational products developed under a NASA-
10 funded project.

11

12 The VIIRS-only product is a statistical regression based on the split window radiances; it suffers from no information
13 about mid- to upper tropospheric moisture. In the VIIRS+NUCAPS operational products, VIIRS IR measurements
14 are merged with CrIS and ATMS water vapor soundings in an earlier attempt to continue the depiction of global
15 moisture at high spatial resolution started with MODIS. The CrIS and ATMS sounding products are provided by the
16 NOAA Unique Combined Atmospheric Processing System (NUCAPS, Gambacorta, 2013). The main idea of merging
17 these products is to capitalize on the unique strengths of each product's spatial and spectral characteristics in the



1 infrared region. VIIRS, with solely the IR window channels, only gives some indication of low-level moisture (which
2 constitutes much of the total column amount) and we complement this with CrIS+ATMS sounding column moisture
3 determinations. This VIIRS+NUCAPS algorithm follows the approach used for MODIS. A clear sky regression
4 relationship is established between TPW and VIIRS IR window brightness temperatures (BTs) and the NUCAPS
5 TPW soundings calculated from a global training radiosonde-based profile data set. A high spatial resolution surface
6 emissivity database (Borbás et al, 2018) is used to help differentiate surface emission and atmospheric moisture
7 absorption. NUCAPS is added in clear and partly cloudy regions to enhance the TPW depiction and to extend the
8 spatial coverage. First, the VIIRS-only clear-sky TPW is generated and stored; subsequently the VIIRS+NUCAPS
9 TPW is calculated in clear-sky conditions. Gaps in the VIIRS+NUCAPS TPW field are filled with adjusted VIIRS-
10 only or adjusted NUCAPS-only products. In this paper we use both the VIIRS-only and VIIRS+NUCAPS total column
11 properties for evaluation.

12

13 Figure 4 shows that the global mean of the TPW derived from the VIIRS+CrIS fusion radiances is found to be 0.3
14 mm too low with a scatter of 3.3 mm when compared to the MYD08 TPW. The VIIRS-only operational TPW are 1.3
15 mm higher than the MYD08 TPW with a scatter of 4.0 mm; much of the VIIRS over-estimation of TPW occurs in the
16 tropical oceans. VIIRS+NUCAPS TPW also performs well with the same 0.3 mm bias, but with a slightly higher 3.5
17 mm scatter in the comparison to MYD08 TPW. However, it does not capture the maxima in the Brazilian rainforest
18 moisture found in the MYD08 TPW. The latitudinal distribution of the differences on Fig. 5 shows good agreement
19 between VIIRS+CrIS fusion and MYD08 and over-estimation of VIIRS-only from 40° S to 10° N latitude. Over the
20 tropics, where the highest moisture levels occur, the VIIRS+CrIS fusion product agrees more closely with the MYD08
21 than the VIIRS+NUCAPS, which mostly underestimates the water vapor content. For this one day global comparison,
22 providing H₂O fields from fusion bands can be regarded as a success for bringing VIIRS+CrIS TPW into family with
23 MYD08 TPW with a slightly better agreement than with the VIIRS+NUCAPS product, and additionally providing a
24 significant improvement over the VIIRS-only product.

25

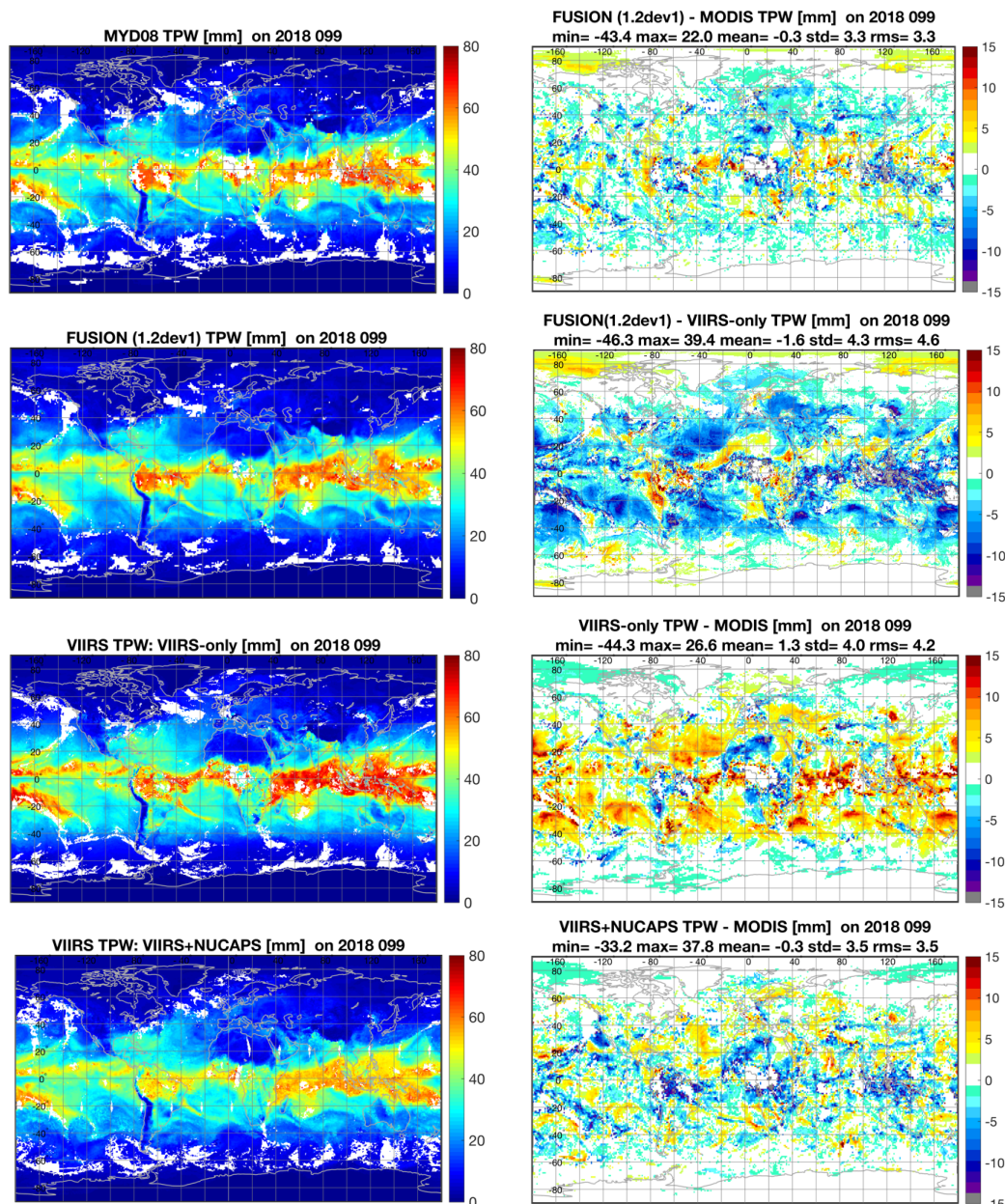
26

27

28

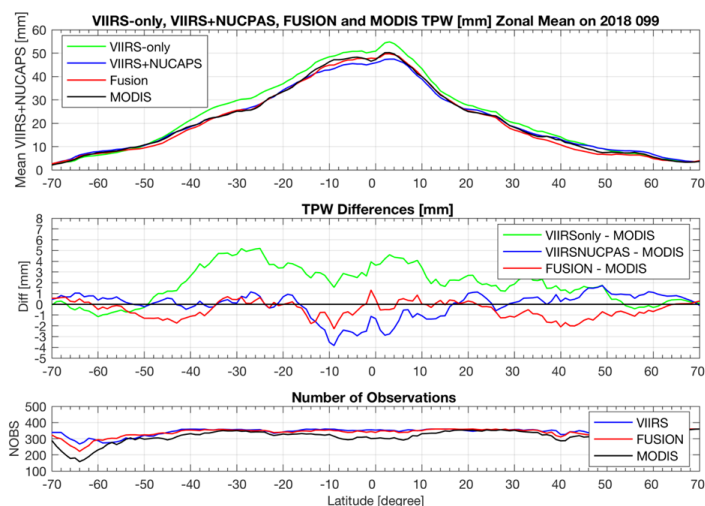
29

30



1 Figure 4. Left: geographical distribution of TPW [mm] results derived from the MODIS MYD08_D3 Collect 6 (left top),
2 VIIRS/CrIS fusion (left second), VIIRS-only (left third) and the VIIRS+NUCAPS (bottom) products for 9 April 2018. The
3 right panels show the corresponding difference fields with their statistics, such as, the minimum (min), maximum (max),
4 mean, standard deviation (std) and root mean square (rms) differences are included in the subtitles.

5



1
2 **Figure 5. Top: latitudinal distribution of TPW [mm] results for the same day and products as on Figure 4 . The middle**
3 **panel illustrates the corresponding differences while the third panel shows the number of observations occurred in each**
4 **one-degree latitude bins.**

5

6 The one day comparisons are now extended to monthly comparisons. Figure 6 shows zonal scatter plots for the month
7 of April 2017 of VIIRS+CrIS fusion, VIIRS-only, and VIIRS+NUCAPS TPW, each with respect to MYD08. The
8 segmentation is into three zones of 60° to 30° N (northern mid-latitudes), 30° N to 30° S (tropics), and 30° to 60° S
9 latitudes (southern mid-latitudes). VIIRS+CrIS fusion TPW shows differences in all three zones in the mean (-1.16,
10 0.24, -0.49 mm respectively) and standard deviation (0.95, 1.89, and 0.66 mm respectively); the dry bias is greater
11 than 1 mm in the northern mid latitudes and is pervasive in the eastern U.S., the northern Atlantic Ocean, through
12 Europe, and continuing to western Russia. Overall good agreement is found in dry (less than 5 mm) as well as wet
13 (greater than 60 mm) atmospheres. Similar comparisons are less favorable for VIIRS-only and VIIRS+NUCAPS,
14 with the exception of northern mid-latitude where VIIRS+NUCAPS shows a smaller absolute bias in the mean of 0.92
15 mm.

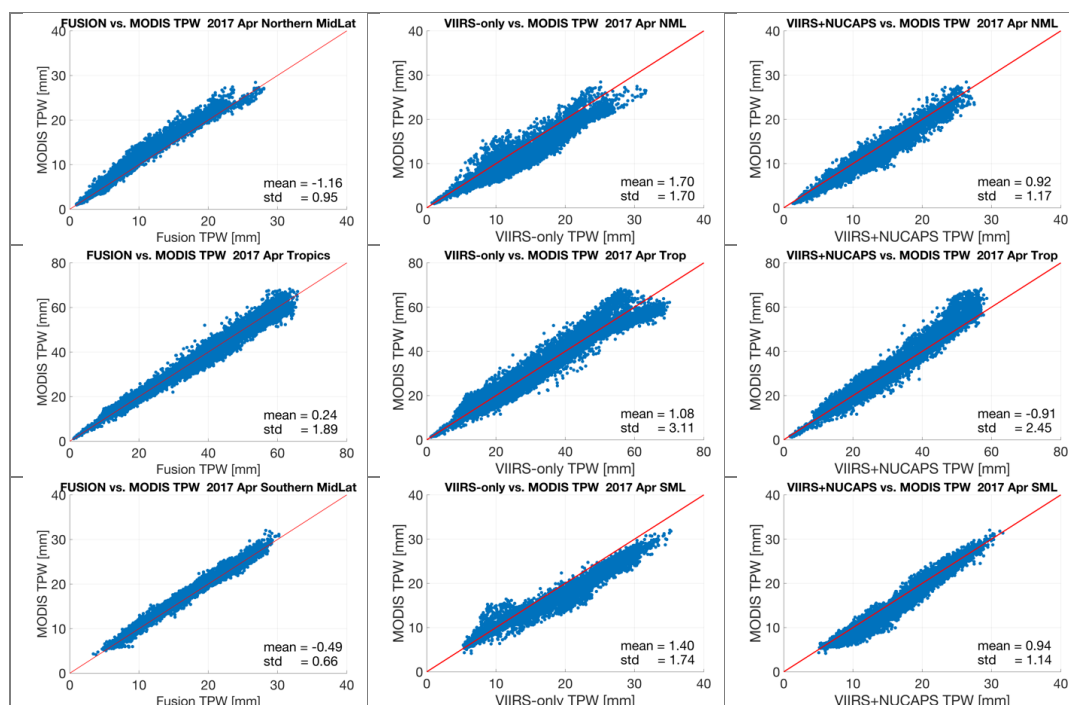
16

17

18

19

20



1

2 **Figure 6. TPW scatter plot of VIIRS+CrIS fusion (left), VIIRS-only (middle) and VIIRS+NUCAPS (right) versus MODIS**
3 **MYD08_M3 Col6.1 for Northern mid latitudes between 30° and 60° N (top), Tropics between 30°S and 30° N (middle), and**
4 **Southern mid latitudes between 30° and 60°S (bottom) on April 2017.**

5

6 Figures 7 and 8 show the global comparison of monthly differences for January 2017. These results reinforce the one
7 day results, especially with regard to VIIRS+CrIS TPW being the best match of the three VIIRS derived TPWs with
8 MYD08 TPW; VIIRS+CrIS has the lowest mean difference at 0.2 mm and standard deviation of 1.4 mm compared to
9 respectively 1.1 and 2.7 mm for VIIRS alone and 0.3 and 2.0 mm for VIIRS+NUCAPS. The improvement is most
10 noticeable (see Fig. 8) over the Brazilian rain forest and the ITCZ (Inter Tropical Convergence Zone).

11

12

13

14

15

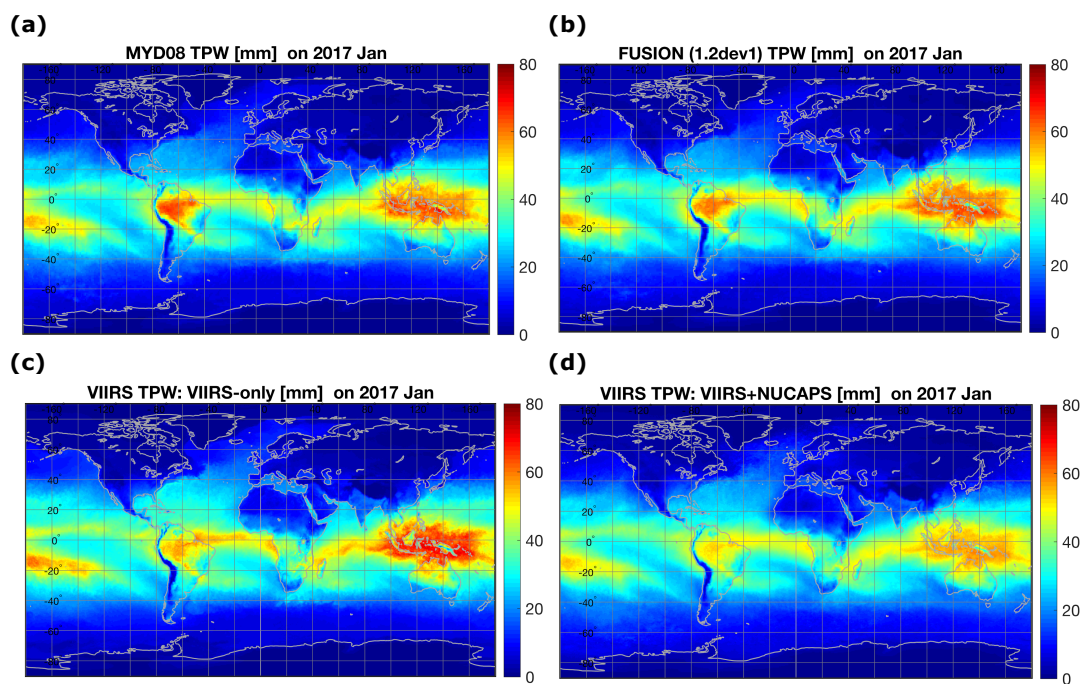
16

17

18

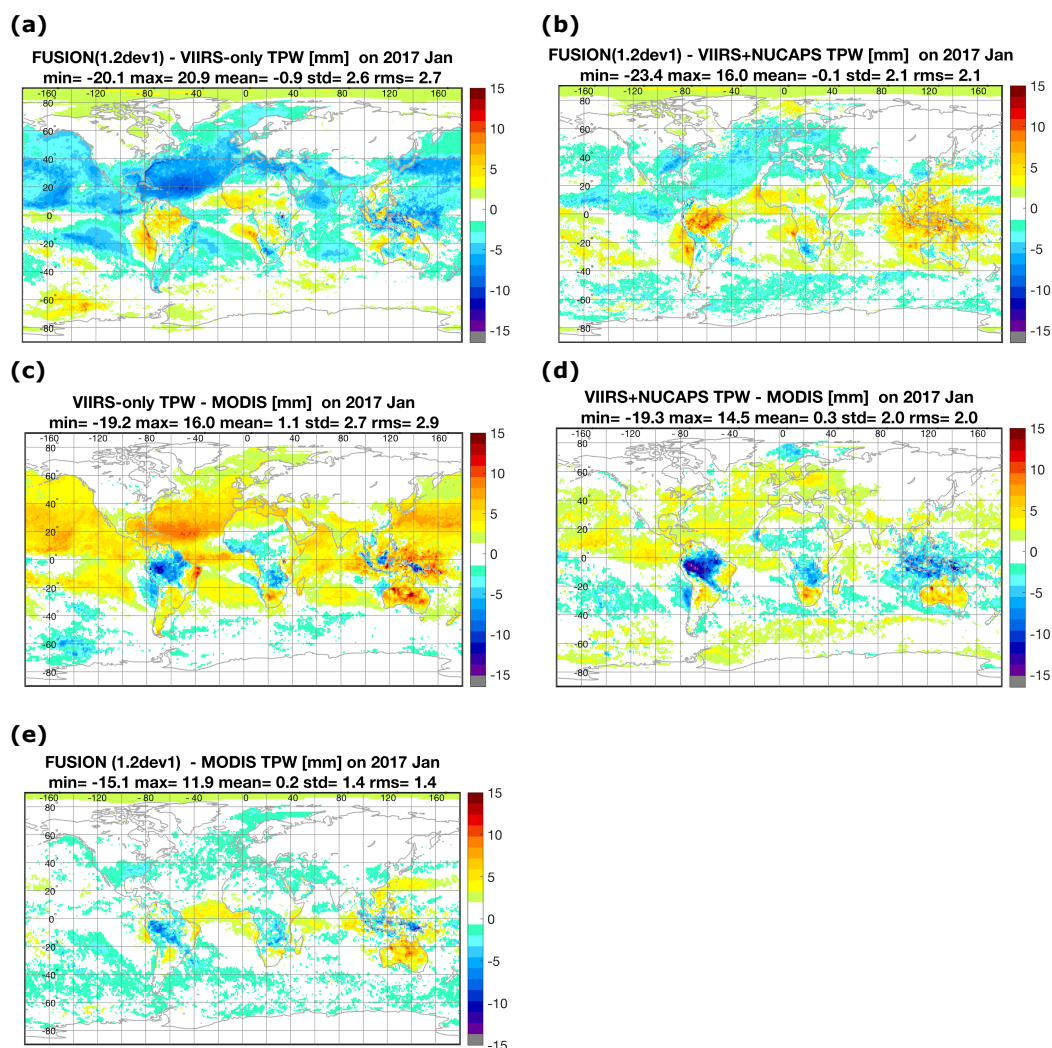
19

20



1 Figure 7. January 2017 geographical distribution of TPW [mm] results derived from the (a) MODIS MYD08_M3 Collect
2 6.1, (b) VIIRS/CrIS fusion, (c) VIIRS-only, and (d) VIIRS+NUCAPS.

3
4
5
6
7
8
9
10
11
12
13
14
15
16
17
18



1 **Figure 8. January 2017 TPW [mm] difference fields of VIIRS+CrIS fusion minus VIIRS-only (a), VIIRS+CrIS fusion minus**
2 **VIIRS+NUCAPS (b), VIIRS-only minus MODIS (c), VIIRS+NUCAPS minus MODIS (d), and VIIRS/CrIS fusion minus**
3 **MODIS. MODIS refers to MYD08_M3 C6.1 products. Minimum (min), maximum (max), mean, standard deviation (std)**
4 **and root mean square (rms) differences are shown in the title.**

5

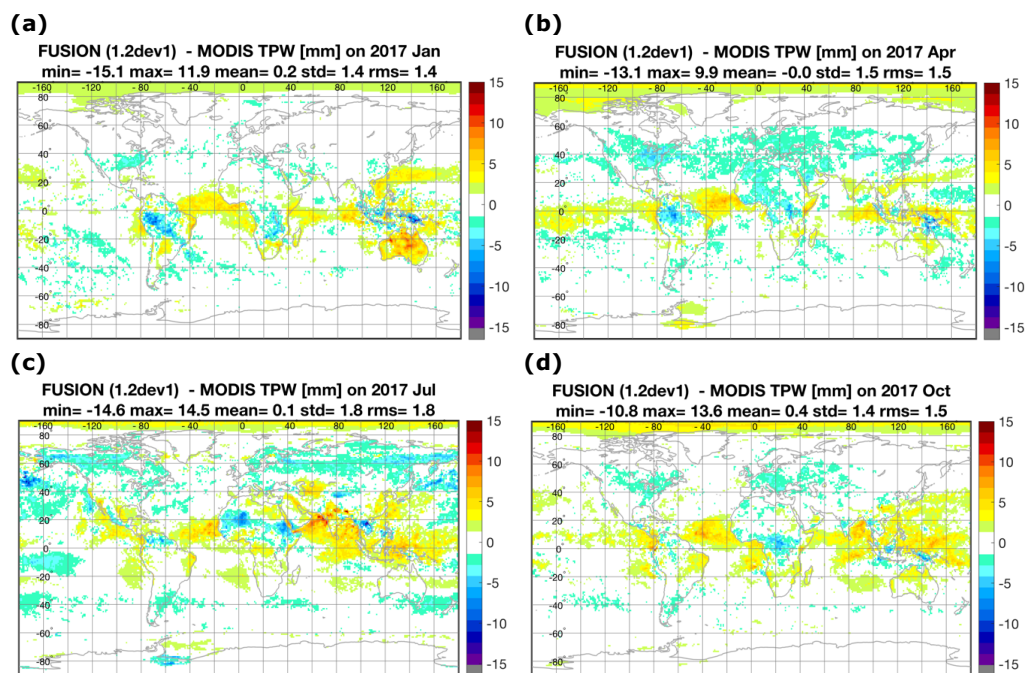
6

7 To extend this analysis to a four season evaluation, VIIRS+CrIS TPW differences with respect to MYD08 TPW are
8 shown for January, April, July, and October 2017 in Fig. 9. Mean agreement ranges from 0.0 mm in April and 0.4
9 mm in October; the standard deviation is largest in July at 1.8 mm. Local VIIRS+CrIS overestimations occur over
10 Australian deserts in January and during the Indian monsoon in July; underestimation is found in the Brazilian
11 rainforest and the ITCZ in January and the Saharan desert in July. In over 300 collocations, MYD08 TPW were
12 compared to ground based microwave radiometer determinations of TPW and found to be dry biased by 0.9 mm with



1 a rms of 3.2 mm (Borbas et al., 2011). In light of this, the overall VIIRS+CrIS TPW agrees very well with MODIS
2 TPW for all four months representing the four seasons.

3



4

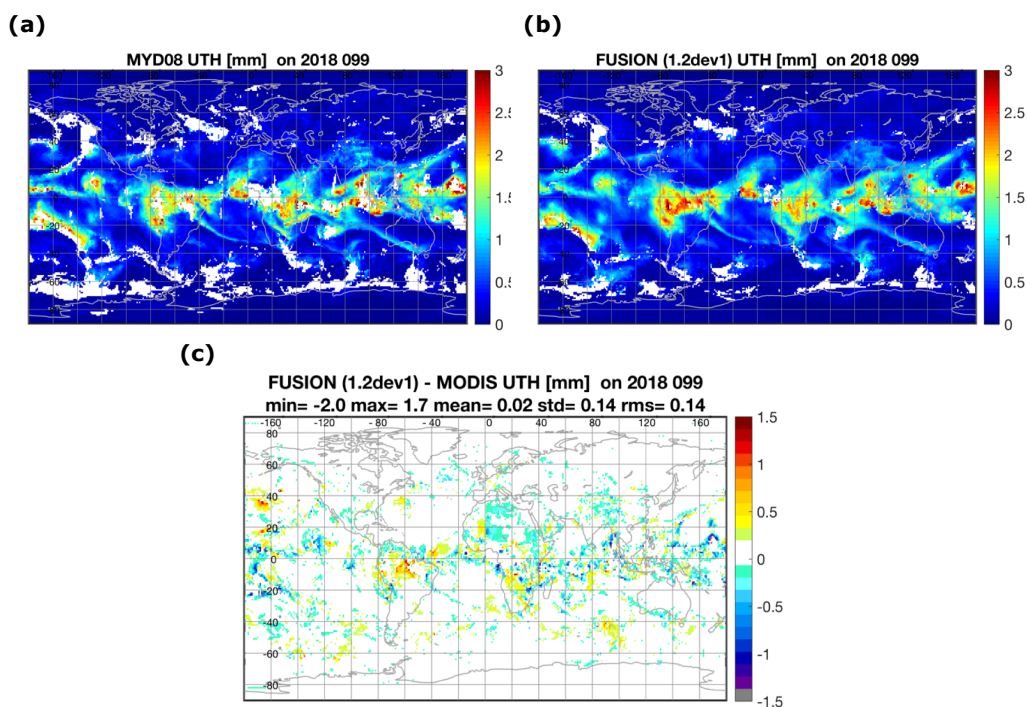
5 **Figure 9.** Geographical distribution of TPW [mm] differences between the VIIRS+CrIS fusion and the MODIS MYD08_M3
6 Collect 6.1 products for (a) January, (b) April, (c) July, and (d) October 2017 representing the four seasons. Minimum
7 (min), maximum (max), mean, standard deviation (std) and root mean square (rms) differences are shown in the title.

8

9 3b. UTH Results

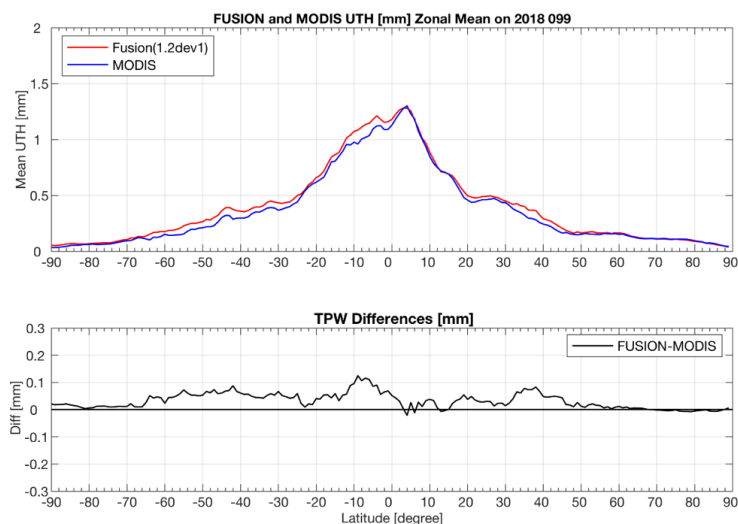
10 Figure 10 shows the results for the VIIRS+CrIS fusion UTH product. The UTH global images on the top two panels
11 show the spatial distribution of UTH within the 0-3 mm range. Here the global mean derived from the VIIRS+CrIS
12 fusion radiances is found to be 0.02 mm higher with a scatter of 0.14 mm when compared to the MYD07 UTH. Local
13 differences of ± 1 mm are found in the tropics. The latitudinal distribution of the differences (Fig. 11) shows modest
14 overestimation in the VIIRS+CrIS fusion UTH everywhere with a peak from 10°S to the equator. Note that the
15 operational VIIRS moisture products do not currently include the UTH product, but only total column moisture
16 information, since VIIRS has a limited ability to sense the upper tropospheric moisture. Again, in this global
17 comparison for one day, use of the H₂O fusion bands brings VIIRS+CrIS fusion UTH into family with MYD08 UTH.
18 Without the fusion radiances, VIIRS has little or no sensitivity to UTH.

19



1

2 **Figure 10.** Geographical distribution of UTH [mm] results derived from the MODIS Collect 6 (a), and VIIRS/CrIS fusion
 3 (b), and their difference (c) for 9 April 201. The minimum (min), maximum (max), mean, standard deviation (std) and root
 4 mean square (rms) differences are shown in the title.

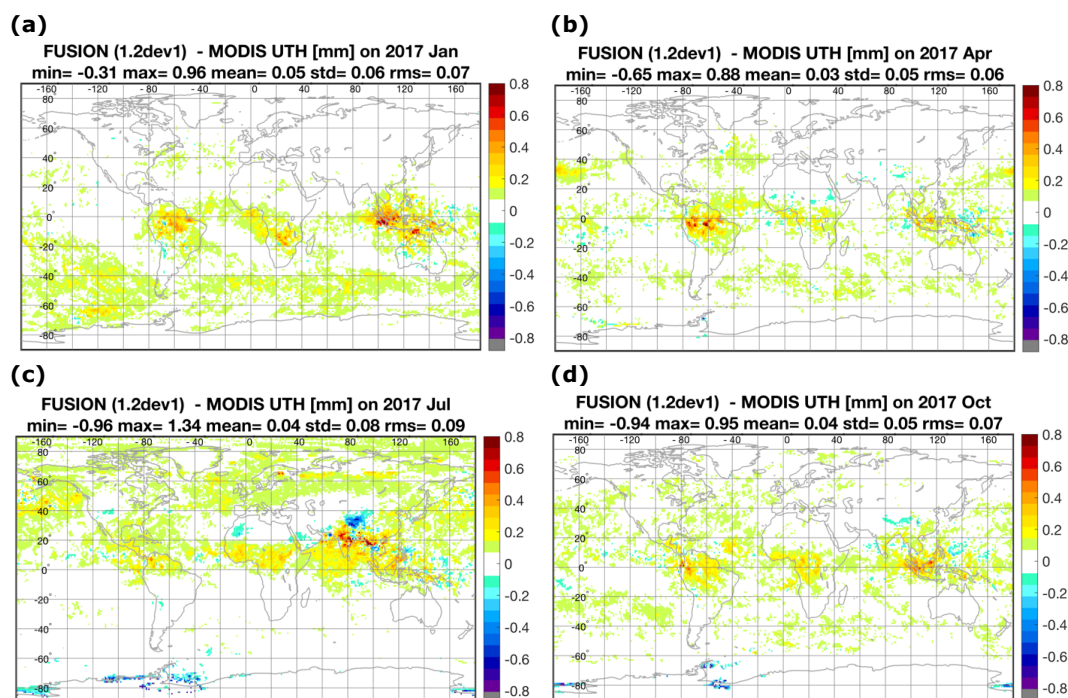


5

6 **Figure 11.** Top: latitudinal distribution of UTH [mm] results for MODIS and VIIRS+CrIS Fusion derived from the same
 7 9 April 2018 data shown in Figure 10. The bottom panel illustrates the corresponding differences. The number of
 8 observations found in each one-degree latitude bins is shown in the bottom panel of Figure 5.



1 Figure 12 shows the UTH comparison results for one month in each season that complement the TPW results in Fig.
2 9. Mean agreement for VIIRS+CrIS UTH with MODIS UTH ranges from 0.03 to 0.56 mm and standard deviation
3 from 0.05 to 0.08 mm. Greatest local differences are found with VIIRS+CrIS too wet in the ITCZ in January, too wet
4 in the Brazilian rain forest in April, too dry in the Himalayas and too wet in India in July, and again too wet in the
5 ITCZ in October. Overall, the results are typically within 10% of each other and accurate enough to determine daily
6 and seasonal variability.
7



8 Figure 12. Same as Figure 9, but for UTH.

9 4. Summary and Conclusions

10 The absence of water vapor and CO₂ absorption IR spectral bands on the VIIRS imager on the Suomi-NPP and NOAA-
11 20 polar-orbiting platforms limits the capability for tropospheric moisture retrievals, especially for upper tropospheric
12 moisture. This study shows the advantage of using IR absorption bands 4.5, 6.7, 7.3, 13.3, 13.6, 13.9, and 14.2 μm that
13 are constructed at VIIRS spatial resolution (750m) using a data fusion approach using both sounder (CrIS) and imager
14 (VIIRS) measurements following the approach in Weisz et al. (2017). The positive impact of adding the constructed
15 fusion spectral bands on TPW and UTH retrievals is demonstrated. The moisture retrievals are based on the MODIS
16 MYD07 Collection 6.1 algorithm package. Evaluation of the resulting moisture products are performed through
17 comparisons to the operational MODIS Collection 6.1 and VIIRS (VIIRS-only and VIIRS+NUCAPS) version 1.0
18 moisture products.



1

2 Improvements in VIIRS+CrIS products, enabled by addition of fusion radiances, over the VIIRS-only and
3 VIIRS+NUCAPS products are observed for TPW when quantitatively compared to the MYD08 products. In our one
4 month study for January 2017, the global mean of the TPW derived from the VIIRS+CrIS fusion radiances is 0.2 mm
5 higher with a scatter of 1.4 mm when compared to the MYD08 TPW; without the fusion radiances (VIIRS-only
6 product) the mean is 1.1 mm too high with a scatter of 2.7 mm with most of the over-estimation occurring in the
7 tropics. The VIIRS+CrIS fusion TPW also demonstrates improvement over the VIIRS+NUCAPS TPW (with 0.3 mm
8 mean and 2.0 mm scatter with respect to the MYD08 product). Similar TPW results are also found for one month in
9 each season of 2017. VIIRS+CrIS UTH, now possible with the addition of the fusion radiances, is found to be within
10 10% of the MYD08 UTH in mean and scatter for the same four months.

11

12 The results in this study are limited to a VIIRS sensor scan angle of 50° to minimize the impact of the CrIS swath
13 being less than that of the imager. These findings are limited in scope but clearly demonstrate the potential in the use
14 of the fusion IR absorption spectral bands in generating moisture products and continuing the moisture record from
15 MODIS and the previous generations of polar orbiting satellite sensors. In future work, we plan to extend this
16 evaluation to longer time periods and possibly replace the operational VIIRS+NUCAPS moisture products with the
17 VIIRS+CrIS fusion derived moisture products.

18

19 **Data availability.** The VIIRS/SNPP Cloud Mask, fusion, water vapor (WATVP) products and the Level-3 MODIS
20 MYD08 products used in this study can be obtained from the NASA Level1 and Atmosphere Archive & Distribution
21 System (LAADS) Distributed Active Archive Center (DAAC), Goddard Space Flight Center, USA.
22 (<https://ladsweb.modaps.eosdis.nasa.gov/search/>)

23

24 **Competing Interests.** The authors declare that they have no conflict of interest.

25 **Author Contributions.** E. Eva Borbas conceived and designed the TPW regression method, conducted the impact
26 study and performed the analyses. Chris Moeller performed the fusion radiance validation in Sect.2. W. Paul Menzel
27 and Bryan A. Baum made critical suggestions on the design of the study and significant improvements to the
28 manuscript. Elisabeth Weisz provided expertise on the use of fusion products.

29 Acknowledgements

30 The authors gratefully acknowledge support from NASA grants 80NSSC18K0816 and 80NSSC18K0816. We are
31 grateful for the encouragement and support by Dr. Hal Maring (NASA Headquarters, Washington, DC). The fusion
32 data are generated by the Atmosphere SIPS at University of Wisconsin – Madison and sent to LAADS for public
33 distribution. The writing of this paper benefited from discussions with our colleague Richard Frey for his insight with
34 the VIIRS cloud mask. We thank Pascal Brunel (Meteo-France) for providing the spectrally shifted MODIS
35 coefficients for RTTOV, Geoff Cureton and Ethan Nelson for their efforts at the A-SIPS and Bhaskar Ramachandran



1 for help in staging the fusion product at LAADS.

2 **References**

- 3 Ackerman, S., et al.: VIIRS/SNPP Cloud Mask and Spectral Test Results 6-min L2 Swath 750m, Version-1. NASA
4 Level1 and Atmosphere Archive & Distribution System (LAADS) Distributed Active Archive Center (DAAC),
5 Goddard Space Flight Center, USA, https://dx.doi.org/10.5067/VIIRS/CLDMSK_L2_VIIRS_SNPP.001, 2019.
6
7 Baum, B. A., et al.: SNPP VIIRS+CrIS Fusion L2 Product. NASA MODIS Adaptive Processing System, Goddard
8 Space Flight Center, USA: https://dx.doi.org/10.5067/VIIRS/FSNRAD_L2_VIIRS_CRIS_SNPP.001, 2019a.
9
10 Baum, B.A., Menzel, W. P., and Weisz E.: Fusion of CrIS and VIIRS data to construct infrared (IR) absorption
11 band radiances for VIIRS, Algorithm Theoretical Basis Document, V1.0
12 <https://ladswb.modaps.eosdis.nasa.gov/missions-and-measurements/viirs/VIIRSCrISFusionATBDv1.1.pdf>, 2019b.
13
14 Borbas, E., Seemann, S. W., Huang, H.-L., Li, J., and Menzel, W. P.: Global profile training database for satellite
15 regression retrievals with estimates of skin temperature and emissivity. Proc. of the Int. ATOVS Study Conference-
16 XIV, Beijing, China, 25-31 May 2005, pp763-770. 2005.
17
18 Borbas, E., Seemann, S. W., Kern, A., Moy, L., Li, J., Gumley, L., and Menzel W.P.: MODIS Atmospheric Profile
19 Retrieval - ATBD. (Collection 006) Products: 07_L2. [https://atmosphere-](https://atmosphere-imager.gsfc.nasa.gov/sites/default/files/ModAtmo/MOD07_atbd_v7_April2011_0.pdf)
20 [imager.gsfc.nasa.gov/sites/default/files/ModAtmo/MOD07_atbd_v7_April2011_0.pdf](https://atmosphere-imager.gsfc.nasa.gov/sites/default/files/ModAtmo/MOD07_atbd_v7_April2011_0.pdf), 2011.
21
22 Borbas, E. E., Seemann, S. W., Li, Z., Li, J., Kern, A., and Menzel, W. P.: MODIS Atmosphere Profiles Product
23 (07_L2). NASA MODIS Adaptive Processing System, Goddard Space Flight
24 Center http://dx.doi.org/10.5067/MODIS/MYD07_L2.006 (Aqua), 2016.
25
26 Borbas, E. E.; Hulley, G., Feltz, M., Knuteson, R., and Hook S.: The Combined ASTER MODIS Emissivity over
27 Land (CAMEL) Part 1: Methodology and High Spectral Resolution Application. Remote Sens.2018, 10, 643.
28 ; <https://doi.org/10.3390/rs10040643>. 2018.
29
30 Borbas, E. E., Li, Z., Menzel, W. P., Dobor L., and Rada M.: VIIRS/Suomi-NPP Water Vapor Products; Algorithm
31 Theoretical Basis Document. [https://ladswb.modaps.eosdis.nasa.gov/missions-and-](https://ladswb.modaps.eosdis.nasa.gov/missions-and-measurements/viirs/SNPPVIIRSWATVP001ATBD2019.pdf)
32 [measurements/viirs/SNPPVIIRSWATVP001ATBD2019.pdf](https://ladswb.modaps.eosdis.nasa.gov/missions-and-measurements/viirs/SNPPVIIRSWATVP001ATBD2019.pdf), 2019a.
33



- 1 Borbas, E. E., Li, Z., Menzel, W. P., Dobor L., and Rada, M.: VIIRS/Suomi-NPP Water Vapor Products (WATVP)
2 Users' Guide; [https://ladsweb.modaps.eosdis.nasa.gov/missions-and-](https://ladsweb.modaps.eosdis.nasa.gov/missions-and-measurements/viirs/SNPPVIIRSWATVP001UserGuide2019.pdf)
3 [measurements/viirs/SNPPVIIRSWATVP001UserGuide2019.pdf](https://ladsweb.modaps.eosdis.nasa.gov/missions-and-measurements/viirs/SNPPVIIRSWATVP001UserGuide2019.pdf), 2019b.
4
5 Borbas, E. E., et al.: VIIRS/SNPP Level-2 Water Vapor Products. NASA MODIS Adaptive Processing System,
6 Goddard Space Flight Center, USA: https://dx.doi.org/10.5067/VIIRS/WATVP_L2_VIIRS_SNPP.001, 2019c.
7
8 Borbas, E. E., et al.: VIIRS/SNPP Level-3 Daily and Monthly Mean Water Vapor Products. NASA MODIS
9 Adaptive Processing System, Goddard Space Flight Center, USA:
10 https://dx.doi.org/10.5067/VIIRS/WATVP_D3_VIIRS_SNPP.001
11 https://dx.doi.org/10.5067/VIIRS/WATVP_M3_VIIRS_SNPP.001, 2019d.
12
13 Gambacorta, A.: The NOAA Unique CrIS/ATMS Processing System (NUCAPS): Algorithm Theoretical Basis
14 Document, <https://pdfs.semanticscholar.org/8f02/7a6e31d08e299c4b79433ee4302b7a8d62cd.pdf>, 2013.
15
16 Hayden, C. M.: GOES-VAS simultaneous temperature-moisture retrieval algorithm. *J. Appl. Meteor.*, 27, 705-733,
17 1988.
18
19 Li, J., Wolf, W., Menzel, W. P., Zhang, W., Huang, H.-L., and Achtor T. H.: Global soundings of the atmosphere
20 from ATOVS measurements: The algorithm and validation, *J. Appl. Meteorol.*, 39: 1248– 1268, 2000.
21
22 Platnick, S., et al.: MODIS Atmosphere L3 Daily Product. NASA MODIS Adaptive Processing System, Goddard
23 Space Flight Center, USA: http://dx.doi.org/10.5067/MODIS/MYD08_D3.006, 2015
24
25 Saha, S., Moorthi, S., Pan, H., Wu, X., and Wang, J.: The NCEP Climate Forecast System Reanalysis. *Bulletin of*
26 *the American Meteorological Society*, 91, 1015–1057, doi:10.1175/2010BAMS3001.1, 2010.
27
28 Saunders, R., Hocking, J., Turner, E., Rayer, P., Rundle, D., Brunel, P., Vidot, J., Roquet, P., Matricardi, M., Geer,
29 A., Bormann, N., and Lupu, C.: An update on the RTTOV fast radiative transfer model (currently at version 12),
30 *Geosci. Model Dev.*, 11, 2717-2737, <https://doi.org/10.5194/gmd-11-2717-2018>, 2018.
31
32 Seemann, S. W., Li, J., Menzel, W. P., and Gumley, L. E.: Operational retrieval of atmospheric temperature,
33 moisture, and ozone from MODIS infrared radiances. *J. Appl. Meteor.*, 42, 1072 1091, 2003.
34
35 Seemann, S. W., Borbas, E.E., Knuteson, R.O., Stephenson, G.R., and Huang, H-L.: Development of a global
36 infrared emissivity database for application to clear sky sounding retrievals from multi-spectral satellite radiances
37 measurements. *J. Appl. Meteorol. and Clim.* 47, 108-123, 2008.



- 1
2 Smith, W. L., and Woolf, H. M.: A Linear Simultaneous Solution for Temperature and Absorbing Constituent
3 Profiles from Radiance Spectra. Technical Proceedings of the Fourth International TOVS Study Conference held in
4 Igls, Austria 16 to 22 March 1988, W. P. Menzel Ed., 330-347, 1988.
5
6 Smith, W. L., et al.: Dual-regression retrieval algorithm for real-time processing of satellite ultraspectral radiances,”
7 J. Appl. Meteorol. Climatol. 51, 1455–1476, 2012.
8
9 Weisz, E., Smith, W. L. Sr., and Smith, N.: Advances in simultaneous atmospheric profile and cloud parameter
10 regression based retrieval from high spectral resolution radiance measurements,” J. Geophys. Res. Atmos. 118(12),
11 6433–6443, 2013.
12
13 Weisz, E., Baum, B. A., and Menzel, W. P.: Fusion of Satellite-Based Imager and Sounder Data to Construct
14 Supplementary High Spatial Resolution Narrowband IR Radiances. J. of Applied Remote Sensing, 11(3), 036022
15 (2017). <https://doi.org/10.1117/1.JRS.11.036022>, 2017.
16